Data Repository items for: Huppert, Perron, & Ashton - The influence of wave power on bedrock seacliff erosion in the Hawaiian Islands

Island vertical motion due to plate migration over the Hawaiian Swell

To account for changes in relative sea level due to island migration over the Hawaiian Swell with Pacific Plate motion we assumed that swell topography remains constant in time as the lithosphere migrates over it, and we tracked changes in swell elevation at each site using a constant azimuth (304° east of north) and plate velocity (92 mm/yr; Morgan and Morgan, 2007). We estimated the topography of the Hawaiian Swell by filtering the bathymetry surrounding the islands with a median filter (Huppert et al., 2015). We used a 480 km x 480 km window size, which maximizes the mean amplitude of the residual topography within the region bound by its zero contour (Wessel, 1998).

Island vertical motion due to volcanic loading

To estimate past changes in relative sea level at each site due to volcanic loading (RSL_v, in meters above present sea level), we compiled radiometric flow ages and drowned coral reef chronostratigraphy to construct a timeline of shield-building volcanism for all volcanoes active during coastal profile evolution (Fig. 3A, Table DR2). Unfortunately, the short historic record of volcanism, challenges associated with radiometric dating of young tholeiitic basalts, and the inaccessibility of the majority of a volcanic edifice below sea level make it difficult to determine the changing loci and rates of volcanic growth over the course of a Hawaiian volcano's construction (Lipman, 1995). Thus, we used the duration of shield building volcanism *T* and the total deflection resulting from loading of each volcano at each coastal profile site w_{tot} (e.g, along the Hāmākua coast of the Big Island, Fig. 3A) to define a range of possible RSL_v timeseries (Fig. 3B). We constructed these by taking the sum of:

$$w(t) = \begin{cases} w_{tot} \cdot \left[1 + \mathrm{erf}\left(\frac{t}{(1-K)T}\right) - \mathrm{erf}\left(\frac{2T-t}{(1-K)T}\right)\right] & K \geq 0 \\ w_{tot} \cdot \left[\mathrm{erf}\left(\frac{T+t}{(K+1)T}\right) - \mathrm{erf}\left(\frac{T-t}{(K+1)T}\right)\right] & K < 0 \end{cases} \tag{DR1}$$

where erf(·) is the error function, *w* is the displacement at a particular site due to loading of a particular volcano at time *t* since the onset of the volcano's shield building, and *K* is an adjustable parameter governing the time-varying displacement rate. Under this formulation, displacement due to loading of a particular volcano can range from instantaneous displacement at the onset of shield building (K = 1) to displacement at a constant rate over the duration of shield building (K = 0) to instantaneous displacement at the end of shield building (K = -1).

Glacio-eustatic sea level change

We assumed that glacio-eustatic sea level varies as implied by the linear transformation of a planktonic $\delta^{18}O$ record from the Cocos Ridge, east equatorial Pacific Ocean, adjusted for temperature changes based on Mg/Ca ratios, over the past 361 ka (Lea et al., 2002) and by linear transformation of a benthic $\delta^{18}O$ record from the East Pacific Rise over the preceding ~1 Ma (Mix et al., 1995; Miller et al., 2005).

Model discretization

We modeled coastal profile evolution assuming that cliff retreat proceeds at a constant lateral rate and that all bedrock undercut by cliff retreat is swiftly evacuated from the coastal zone. Initializing the models at the paleoprofile reconstructions, discretized vertically with one meter elevation spacing, we assumed that lateral erosion occurs at the node on the profile at or immediately below relative sea level at each time step. All topography undercut by coastal incision is removed, generating a vertical cliff at the coast. We varied relative sea level every 1 kyr based on the sum of the relative sea level change due to glacio-eustasy, island migration over the Hawaiian Swell, and volcanic loading.

Model evaluation

We constructed possible RSL_v for a range of effective elastic thicknesses of the lithosphere T_e and trends of deflection during shield building prescribed by K. We then added each RSL_v to the vertical motion trend inferred for migration over swell topography at the coastal profile site (Huppert et al., 2015) and an oxygen-isotope based eustatic sea level record (Fig. 3B; Mix et al., 1995; Lea et al., 2002) We cropped each resulting net relative sea level history at the most recent occurrence of sea level at the slope break depth and checked that the implied age is consistent with slope break ages inferred from radiometric dating of dredged basalts and stratigraphic relations between volcanic flows and drowned coral reefs (Fig. 3C, Table DR1).

We tested 600 cliff retreat rates between 0.5 mm/yr and 300 mm/yr for each paleoprofile reconstruction and relative sea level history (15 effective elastic thicknesses of the lithosphere T_e and 20 values of K). To evaluate the goodness of fit between the modeled profiles x_{mod} and the observed profiles x at each elevation node, we calculated the normalized root mean square error:

$$NRMSE = \frac{\sqrt{\frac{1}{N}\sum_{i=1}^{N}\left(x_{model,i} - x_i\right)^2}}{\max(x) - \min(x)} \qquad \text{(DR2)}$$

where N is the number of elevation nodes between the slope break and the observed cliff top.

To determine the relative sea level history (effective elastic thickness of the lithosphere and value of K) best able to reproduce the observed coastal profiles at all of the sites simultaneously, we calculated the average NRMSE of all 11 profiles using the local best-fit cliff retreat rate. We normalized the NRMSE of each profile by the NRMSE of its paleoprofile before taking the average so that more deeply eroded profiles, with greater mismatch between their paleoprofile and observed profile, did not unduly influence selection of the global best-fit relative sea level history. We used this procedure to determine the globally consistent best-fit relative sea level history for the upper bound paleoprofiles, the lower bound paleoprofiles and both paleoprofiles simultaneously (taking the average normalized NRMSE of models initiated from all 22 paleoprofile reconstructions). Through this procedure, we obtained estimates of both the global best-fit relative sea level history and, for a given relative sea level history, the best-fit cliff retreat rates at each site.

We found a consistent best-fit relative sea level history (T_e = 30 km, K = -0.3) using the average normalized NRMSE of only the upper bound paleoprofile models, only the lower bound paleoprofile models, or both paleoprofiles simultaneously.

Wave power calculation

We compared the best-fit retreat rate at each site for the global best-fit relative sea level history to the mean annual wave power and one-year recurrence interval wave power, calculated from hourly hindcast wave data spanning 1980 to 2011 at the Wave Information Studies (WIS) array of virtual buoys surrounding the Hawaiian Islands (Jensen, 2010). The virtual buoy locations are >30 km offshore in waters >1.8 km deep (Fig. 1A). Using the timeseries of significant deep-water wave height H_0, mean wave period T, and vector mean wave direction (relative to the shore-normal direction at a given site) θ_0 at the buoy nearest the site's swath profile, we computed wave power density (kW/m):

$$P = \frac{\rho g^2 H_0^2 T}{16\pi} \cos\theta_0 \quad , \theta_0 < 90° \tag{DR3}$$

and calculated the mean of the hourly observations (including instances of zero wave power when mean wave direction is not directed shorewards) to find the mean annual wave power of the complete 30-year record. To find the one-year recurrence interval wave power, we calculated the recurrence interval of each hourly wave power measurement, (1+M)/r, where M is the number of hourly measurements and r is the rank of the measurement, with r = 1 representing the maximum hourly wave power measured at the buoy. We linearly interpolated to find the one-year recurrence interval wave power from the hourly measurements and recurrence intervals.

References

Bonhommet, N., Beeson, M.H., and Dalrymple, G.B., 1977, A contribution to the geochronology and petrology of the island of Lanai, Hawaii: Geological Society of America Bulletin, v. 88, p. 1282–1286.

Clague, D.A., and Calvert, A.T., 2009, Postshield stage transitional volcanism on Mahukona Volcano, Hawaii: Bulletin of Volcanology, v. 71, p. 533–539.

Garcia, M.O., Hanano, D., Flinders, A., Weis, D., Ito, G., and Kurz, M.D., 2012, Age, geology, geophysics, and geochemistry of Mahukona Volcano, Hawaii: Bulletin of Volcanology, v. 74, p. 1445–1463.

Huppert, K.L., Royden, L.H., and Perron, J.T., 2015, Dominant influence of volcanic loading on vertical motions of the Hawaiian Islands: Earth and Planetary Science Letters, v. 418, p. 149–171.

Jensen, R.E., 2010, Wave Information Studies: US Army Corp of Engineers, https://chl.erdc.dren.mil/cods-wave-measurements/.

Jicha, B.R., Rhodes, J.M., Singer, B.S., and Garcia, M.O., 2012, 40Ar/39Ar geochronology of submarine Mauna Loa volcano, Hawaii: Journal of Geophysical Research: Solid Earth, v. 117.

Jourdan, F., Sharp, W.D., and Renne, P.R., 2012, 40Ar/39Ar ages for deep (3.3 km) samples from the Hawaii Scientific Drilling Project, Mauna Kea volcano, Hawaii: Geochemistry, Geophysics, Geosystems, v. 13.

Lea, D.W., Martin, P.A., Pak, D.K., and Spero, H.J., 2002, Reconstructing a 350 ky history of sea level using planktonic Mg/Ca and oxygen isotope records from a Cocos Ridge core: Quaternary Science Reviews, v. 21, p. 283–293.

Leonhardt, R., McWilliams, M., Heider, F., and Soffel, H., 2009, The Gilsá excursion and the Matuyama/Brunhes transition recorded in 40 Ar/39 Ar dated lavas from Lanai and Maui, Hawaiian Islands: Geophysical Journal International, v. 179, p. 43–58.

Lipman, P.W., 1995, Declining growth of Mauna Loa during the last 100,000 years: Rates of lava accumulation vs. gravitational subsidence: GEOPHYSICAL MONOGRAPH-AMERICAN GEOPHYSICAL UNION, v. 92, p. 45–80.

Lipman, P.W., and Calvert, A.T., 2011, Early growth of Kohala volcano and formation of long Hawaiian rift zones: Geology, v. 39, p. 659–662.

Lipman, P.W., Sisson, T.W., Ui, T., Naka, J., and Smith, J.R., 2002, Ancestral submarine growth of Kilauea volcano and instability of its south flank: GEOPHYSICAL MONOGRAPH-AMERICAN GEOPHYSICAL UNION, v. 128, p. 161–192.

McDougall, I., 1964, Potassium-argon ages from lavas of the Hawaiian Islands: Geological Society of America Bulletin, v. 75, p. 107–128.

Miller, K.G., Kominz, M.A., Browning, J.V., Wright, J.D., Mountain, G.S., Katz, M.E., Sugarman, P.J., Cramer, B.S., Christie-Blick, N., and Pekar, S.F., 2005, The Phanerozoic record of global sea-level change: science, v. 310, p. 1293–1298.

Mix, A., Pisias, N., Rugh, W., Wilson, J., Morey, A., and Hagelberg, T., 1995, 17. Benthic foraminifer stable isotope record from Site 849 (0-5 Ma): local and global climate changes, *in* Proc. Ocean Drill. Program, Sci. Results, v. 138, p. 371–412.

Moore, J.G., and Clague, D.A., 1992, Volcano growth and evolution of the island of Hawaii: Geological Society of America Bulletin, v. 104, p. 1471–1484.

Morgan, W.J., and Morgan, J.P., 2007, Plate velocities in the hotspot reference frame: SPECIAL PAPERS-GEOLOGICAL SOCIETY OF AMERICA, v. 430, p. 65.

Naughton, J., Macdonald, G., and Greenberg, V., 1980, Some additional potassium-argon ages of Hawaiian rocks: the Maui volcanic complex of Molokai, Maui, Lanai and Kahoolawe: Journal of Volcanology and Geothermal Research, v. 7, p. 339–355.

PRISM Climate Group, 2011, PRISM climate model: Oregon State University,.

Sano, H., Sherrod, D.R., and Tagami, T., 2006, Youngest volcanism about 1 million years ago at Kahoolawe Island, Hawaii: Journal of volcanology and geothermal research, v. 152, p. 91–96.

Sherrod, D.R., Murai, T., and Tagami, T., 2007a, New K–Ar ages for calculating end-of-shield extrusion rates at West Maui volcano, Hawaiian island chain: Bulletin of volcanology, v. 69, p. 627–642.

Sherrod, D.R., Sinton, J.M., Watkins, S.E., and Brunt, K.M., 2007b, Geologic map of the State of Hawaii: US geological survey open-file report, v. 1089.

Taylor, B., 2019, Shoreline slope breaks revise understanding of Hawaiian shield volcanoes evolution: Geochemistry, Geophysics, Geosystems, v. 20, p. 4025–4045.

Wessel, P., 1998, An empirical method for optimal robust regional-residual separation of geophysical data: Mathematical Geology, v. 30, p. 391–408.

FIGURE CAPTIONS:

Figure DR1. Swath profiles on the Big Island of Hawaiʻi, Maui, and Kahoʻolawe, labeled as in Fig. 1. C-M: Black line shows mean elevations along profile. Dashed line shows slope break depth. Teal and magenta dashed lines show upper bound (UB) paleoprofile and lower bound (LB) paleoprofile reconstruction, respectively. Solid teal and magenta lines show corresponding best-fit modeled profiles for the best-fit relative sea level history with effective elastic thickness of the lithosphere T_e = 30 km and parameter K = -0.3 (see Equation DR1). Inset map shows swath profile locations.

TABLE CAPTIONS:

Table DR1. Bedrock coastal profiles: geology, mean annual rainfall, and attributes from profile analyses

Table DR2. Duration of shield building estimated from K-Ar and Ar-Ar dating of shield stage basalts and drowned coral reef stratigraphy

Table DR3. Mean annual wave power (± 2 standard deviations of interannual mean annual wave power) and one-year recurrence interval wave power in deep water at the coastal profile sites

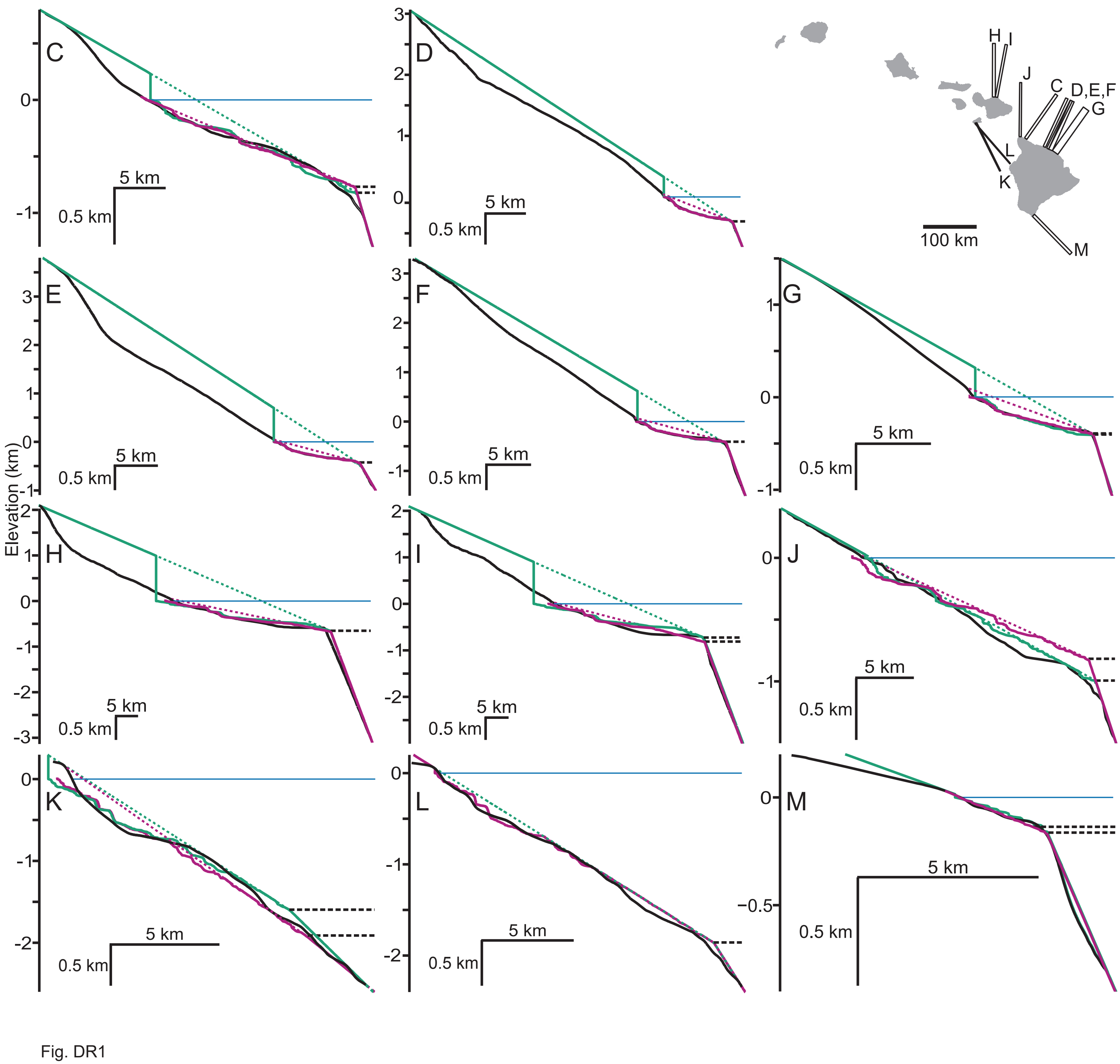

Fig. DR1

Table DR1. Bedrock coastal profiles: geology, mean annual rainfall, and attributes from profile analyses

						Slope break depth (m)			Slope break age (ka)			Seacliff retreat rate (mm/yr)		
Lat (°)	Long (°)	Volcano	Flow unit	Flow type	Bedrock age (ka)[a]	UB	LB	Reported[b]	UB	LB	Reported	UB	LB	Shelf width[†]
18.94	-155.64	Mauna Loa	Kau	Shield	13-50	137	163	150-160	12	14	15[b]	116.5	49	13.8 ±0.3
19.99	-155.23	Mauna Kea	Hāmākua	Postshield	64-300	407	395	350-500	103	94	~130[b,c]	108	132	60.2 ± 0.1
20.03	-155.32	Mauna Kea	Hāmākua	Postshield	64-300	452	406	350-500	130	125	~130[b,c]	111.5	117.5	74.1 ± 0.5
20.06	-155.36	Mauna Kea	Hāmākua	Postshield	64-300	462	424	350-500	133	129	~130[b,c]	111	109	72.6 ± 0.7
20.09	-155.42	Mauna Kea	Hāmākua	Postshield	64-300	405	392	350-500	129	127	~130[b,c]	101.5	100	62.6 ± 0.2
20.23	-155.75	Kohala	Pololū	Shield	320-450	822	769	950-1150	316	300	430[b], $\gtrsim 340$[c]	112	79	81.5 ± 0.5
20.27	-155.86	Kohala	Pololū	Shield	320-450	993	818	950-1150	365	334	430[b], $\gtrsim 340$[c]	76	100.5	79.6 ± 1.7
20.94	-156.27	Haleakalā	Kula	Postshield	150-930	725	811	550-2400	1030	1058	950-1200[b,c]	117	83.5	37.1 ± 0.3
20.94	-156.31	Haleakalā	Kula	Postshield	150-930	651	670	550-2400	1026	1028	950-1200[b,c]	129	105	39.7 ± 0.1
20.51	-156.65	Kaho'olawe	Kanapou	Transitional/ postshield	1100-1400	1858	1858	550-2400	1368	1368	950-1200[b,c]	19	19	17.5 ± 0.0
20.51	-156.57	Kaho'olawe	Kanapou	Transitional/ postshield	1100-1400	1597	1911	550-2400	1278	1360	950-1200[b,c]	19	16.5	12.2 ± 0.6

[a] (Sherrod et al., 2007b) and reference therein, [b] (Taylor, 2019) , [c] (Moore and Clague, 1992)

[†]Uncertainty reflects uncertainty on shelf width and on the age of the volcanic edifice

Table DR2. Duration of shield building estimated from K-Ar and Ar-Ar dating of shield stage basalts and drowned coral reef stratigraphy

Volcano	**Onset of shield building (Ma)**	**End of shield building (Ma)**	**Reference(s)**
Kīlauea	0.23	0	Sherrod et al., 2007b citing Lanphere in Lipman et al., 2002
Mauna Loa	0.66	0	Jicha et al., 2012
Mauna Kea	0.68	0.24	Moore and Clague, 1992; Jourdan et al., 2012
Hualālai	0.75	0.1	Moore and Clague, 1992
Kohala	1.16	0.25	Moore and Clague, 1992; Lipman and Calvert, 2011
Māhukona	0.65	0.30	Clague and Calvert, 2009; Garcia et al., 2012
Haleakalā	1.45	0.95	Moore and Clague, 1992
Kaho'olawe	1.4	1.2	Sherrod et al., 2007b citing Fodor et al., 1992; Sano et al., 2006
West Maui	2.1	1.35	Sherrod et al., 2007b citing McDougall, 1964; Naughton et al., 1980; Sherrod et al., 2007a
Lāna'i	1.60	1.24	Sherrod et al., 2007b citing Bonhommet et al., 1977; Leonhardt et al., 2009

Table DR3. Mean annual wave power (± 2 standard deviations of interannual mean annual wave power) and one-year recurrence interval wave power in deep water at the coastal profile sites

Lat. (°)	Long. (°)	Mean annual wave power (kW/m)	One-year recurrence interval wave power (kW/m)
18.94	-155.64	36.4 ± 5.7	409.9
19.99	-155.23	72.3 ± 7.9	642.2
20.03	-155.32	73.8 ± 9.1	749.7
20.06	-155.36	73.8 ± 8.8	728.8
20.09	-155.42	73.8 ± 9.0	741.6
20.23	-155.75	68.9 ± 7.8	657.8
20.27	-155.86	75.3 ± 15.0	1210.1
20.94	-156.27	77.6 ± 12.3	1018.2
20.94	-156.31	76.7 ± 14.9	1215.5
20.51	-156.65	10.4 ± 1.8	165.8
20.51	-156.57	12.3 ± 2.0	153.6